INTERNATIONAL JOURNAL FOR NUMERICAL METHODS IN FLUIDS
Int. J. Numer. Meth. Fluids 2009; **60**:95–117
Published online 29 July 2008 in Wiley InterScience (www.interscience.wiley.com). DOI: 10.1002/fld.1883

A lattice Boltzmann model for the compressible Euler equations with second-order accuracy

Jianying Zhang, Guangwu Yan*, †, Xiubo Shi and Yinfeng Dong

College of Mathematics, Jilin University, Changchun 130012, People's Republic of China

SUMMARY

In this paper, we propose a new lattice Boltzmann model for the compressible Euler equations. The model is based on a three-energy-level and three-speed lattice Boltzmann equation by using a method of higher moments of the equilibrium distribution functions. In order to obtain second-order accuracy, we employ the ghost field distribution functions to remove the non-physical viscous parts. We also use the conditions of the higher moment of the ghost field equilibrium distribution functions to obtain the equilibrium distribution functions. In the numerical examples, we compare the numerical results of this scheme with those obtained by other lattice Boltzmann models for the compressible Euler equations. Copyright © 2008 John Wiley & Sons, Ltd.

Received 27 March 2007; Revised 10 June 2008; Accepted 10 June 2008

KEY WORDS: lattice Boltzmann method; compressible Euler equations; ghost field

1. INTRODUCTION

The lattice Boltzmann method (LBM) has been developed as an alternative method for computational fluid dynamics. This method originated from a Boolean fluid model known as the lattice gas automata (LGA) [1], which simulates the motion of the fluids by particles moving and colliding on a regular lattice. During the past few years much progress has been made to extend the LBM to become a tool for simulating many complex fluid dynamics problems, such as multi-phase flow, suspension flow and flow in the porous media, which are quite difficult to simulate by conventional methods [2–5]. On the other hand, the LBM has undergone a number of further refinements. A recent series of studies by Yan *et al*. showed that the LBGK model could be used to simulate

*Correspondence to: Guangwu Yan, College of Mathematics, Jilin University, Changchun 130012, People's Republic of China.
†E-mail: yangw@email.jlu.edu.cn

Contract/grant sponsor: Jilin University; contract/grant number: 985 Project
Contract/grant sponsor: National Nature Science Foundation of China; contract/grant numbers: 10072023, 90305013
Contract/grant sponsor: Chuangxin Foundation of Jilin University; contract/grant number: 2004CX041

wave motion [6], soliton waves [7], Lorenz attractor [8], Burgers equation [9] and the Schrödinger equation [10]; other investigators have also studied the Schrödinger equation [11] and Poisson equation [12, 13]. All of these models can be derived by using higher-order moment methods with a multi-scale technique and a series of partial differential equations in different time scales. In this paper, a lattice Boltzmann model for the Euler equations is proposed based on this higher-order moment method.

The LBM starts from the mesoscopic kinetic equation, i.e. the lattice Boltzmann equation governs macroscopic quantities in fluid flows. The kinetic nature has many advantages over conventional numerical methods, such as the algorithmic simplicity, the parallel computation, the easy handling of complex boundary conditions and the efficient hydrodynamics simulations.

A challenging problem is the question of the ability of the LBM to simulate compressible flows. There are a number of lattice Boltzmann models of compressible flows [14–30]. Alexander *et al*. [14] chose a modified equilibrium distribution, allowing a smaller sound speed. Nadiga [15] proposed a discrete velocity model. Huang *et al*. [16] used a method with flow-adapted discrete velocities, a non-unique equilibrium distribution constrained by a set of linear moments and the use of interpolated nodes. Prendergast and Xu [17], Kim *et al*. [18] and Kotelnikov and Montgomery [19] used Bhatnagar–Gross–Krook-type models to establish a new type of flux and employed TVD flux limitation with the neighboring cells. Renda *et al*. [20], Vahala *et al*. [21], Sun [22], De Cicco *et al*. [23], Mason [24, 25], Kataoka [26, 27] and Yan [28–30] proposed many models by using additional techniques to obtain a higher Mach number for compressible flows.

It is well known that many techniques can be used to simulate the compressible flows [31–35], for example, the finite volume method with unstructured meshes is used to fit complex boundaries [31]; the total variation diminishing (TVD) [32]; the essentially non-oscillatory (ENO) [33] methods are used to minimize numerical diffusions and non-physical oscillatory effects; the meshless method can remove the restrictions of grid meshes [34]; and the level set method can be used to trace moving boundaries [35]. When these schemes are applied to a shock wave tube problem, a very high resolution for the shock will be required, especially in TVD-type schemes. However, the contact discontinuity is still spread over typically three to four grid cells. For the Eulerian finite-difference method, the contact discontinuities are more difficult to compute with high resolution than in the case of a shock, since they do not have a natural compression mechanism to sharpen the numerical resolution. The LBM can offer an ideal numerical effect and a new insight [28]. Here, we focus on the compressible Euler equations and its simulation by using the lattice Boltzmann model.

A fundamental problem needs to be solved in the compressible lattice Boltzmann model, which is how to describe the compressible Euler equations with second-order accuracy in the truncation error. In References [28] and [30], the first-order Euler equations and the second-order Navier–Stokes equations are proposed, respectively. Nevertheless, higher than second-order Navier–Stokes equations contain non-physical viscosity. In fact, these lattice Boltzmann models in References [28, 30] are the first-order Euler equations model. In this paper, the target is to propose a second-order Euler equation model. To solve this problem, a simple strategy is to modify the second-order Navier–Stokes equations model by using a ghost field distribution. The role of the ghost field is to remove the physical viscosity.

The main target of this paper can be divided into two parts: (1) to propose a new lattice Boltzmann model for the second-order compressible Euler equations by using the ghost field and (2) to obtain the equilibrium distribution functions of the ghost field.

DOI: 10.1002/fld

In the next section, the three-energy-level lattice Boltzmann model is described. In Section 3, we contribute the Euler equations by using a ghost field distribution. In Section 4, we simulate some numerical examples by using this lattice Boltzmann model, and Section 5 gives conclusions.

2. LATTICE BOLTZMANN MODEL

2.1. Lattice Boltzmann equation

Let us consider a two-layer one-dimensional lattice with four links that connect the center site to four neighbor nodes on every layer. We assume that the particles moving along the link with velocity $\mathbf{e}_\alpha$ are divided into two kinds, A and B, with different energy levels ε_A ($\alpha=1,\ldots,4$) and ε_B ($\alpha=5,\ldots,8$), and $\alpha=0$ is the rest particles possessing energy level ε_D. Hence, it is actually a nine-bit model with three speeds $0, c, 2c$, where c is the speed of the particles at the face center: $|\mathbf{e}_\alpha|=c$ ($\alpha=1,2,5,6$), $|\mathbf{e}_\alpha|=2c$ ($\alpha=3,4,7,8$) and $|\mathbf{e}_0|=0$; see Figure 1.

We define $F_\alpha(\mathbf{x},t)$ as the distribution function at site $\mathbf{x}$, and time t, with velocity $\mathbf{e}_\alpha$. The distribution function $F_\alpha(\mathbf{x},t)$ consists of two parts: particle distribution function $f_\alpha(\mathbf{x},t)$ and ghost field distribution function $g_\alpha(\mathbf{x},t)$ [36], namely

$$F_\alpha(\mathbf{x},t)=f_\alpha(\mathbf{x},t)+g_\alpha(\mathbf{x},t) \tag{1}$$

The macroscopic quantities of mass, momentum and total energy per site are defined as follows:

$$\rho\equiv\sum_\alpha F_\alpha \tag{2}$$

$$\rho u\equiv\sum_\alpha e_\alpha F_\alpha \tag{3}$$

$$\frac{1}{2}\rho u^2+\rho E\equiv\sum_\alpha F_\alpha\varepsilon_\alpha \tag{4}$$

where E is the internal energy of every unit mass. ε_α is the energy level [28, 30], and it has three numerical values $\varepsilon_A, \varepsilon_B$ and ε_D. The lattice Boltzmann equations are expressed as

$$F_\alpha(\mathbf{x}+\mathbf{e}_\alpha,t+1)=F_\alpha(\mathbf{x},t)-\frac{1}{\tau}[F_\alpha(\mathbf{x},t)-F_\alpha^{\mathrm{eq}}(\mathbf{x},t)] \tag{5}$$

where τ is the single relaxation time, $F_\alpha^{\mathrm{eq}}(\mathbf{x},t)$ is the local equilibrium distribution function at site $\mathbf{x}$, and time t, with velocity $\mathbf{e}_\alpha$.

We assume that the equilibrium distribution function $F_\alpha^{\mathrm{eq}}(\mathbf{x},t)$ is the sum of two parts

$$F_\alpha^{\mathrm{eq}}=f_\alpha^{\mathrm{eq}}+g_\alpha^{\mathrm{eq}} \tag{6}$$

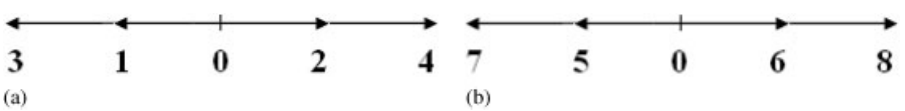

Figure 1. Schematic diagram of lattice, (a) type A and (b) type B.

DOI: 10.1002/fld

and meets the conservation conditions

$$\sum_{\alpha} F_{\alpha}^{\mathrm{eq}} = \rho \tag{7}$$

$$\sum_{\alpha} e_{\alpha} F_{\alpha}^{\mathrm{eq}} = \rho u \tag{8}$$

$$\sum_{\alpha} F_{\alpha}^{\mathrm{eq}} \varepsilon_{\alpha} = \frac{1}{2}\rho u^2 + \rho E \tag{9}$$

In Equation (6), $f_{\alpha}^{\mathrm{eq}}(\mathbf{x}, t)$, $g_{\alpha}^{\mathrm{eq}}(\mathbf{x}, t)$ are the local equilibrium distribution function and the local ghost field equilibrium distribution function at site $\mathbf{x}$, and time t, with velocity $\mathbf{e}_{\alpha}$. The local ghost field equilibrium distribution function $g_{\alpha}^{\mathrm{eq}}(\mathbf{x}, t)$ is given in the next section. We assume that f_{α}^{eq} has the following form:

$$\begin{aligned}
f_{\alpha}^{\mathrm{eq}} &= A_0'\rho + A_2'\rho u e_{\alpha} + A_6'\rho u^2 + A_7'\rho u^3 e_{\alpha}^3 \quad (\alpha = 1, 2), \quad \varepsilon_{\alpha} = \varepsilon_A \\
f_{\alpha}^{\mathrm{eq}} &= A_0''\rho + A_2''\rho u e_{\alpha} + A_6''\rho u^2 + A_7''\rho u^3 e_{\alpha}^3 \quad (\alpha = 3, 4), \quad \varepsilon_{\alpha} = \varepsilon_A \\
f_{\alpha}^{\mathrm{eq}} &= B_0'\rho + B_2'\rho u e_{\alpha} + B_6'\rho u^2 + B_7'\rho u^3 e_{\alpha}^3 \quad (\alpha = 5, 6), \quad \varepsilon_{\alpha} = \varepsilon_B \\
f_{\alpha}^{\mathrm{eq}} &= B_0''\rho + B_2''\rho u e_{\alpha} + B_6''\rho u^2 + B_7''\rho u^3 e_{\alpha}^3 \quad (\alpha = 7, 8), \quad \varepsilon_{\alpha} = \varepsilon_B \\
f_0^{\mathrm{eq}} &= D_0\rho + D_6\rho u^2 \quad (\alpha = 0), \quad \varepsilon_{\alpha} = \varepsilon_D
\end{aligned}$$

where coefficients A_{β}', A_{β}'', B_{β}', B_{β}'' ($\beta = 0, 2, 6, 7$), D_{β} ($\beta = 0, 6$) are determined by a set of reasonable requirements. These requirements consist of the conservation laws of mass, momentum, energy and the conditions of the higher-order moments [30]:

$$\sum_{\alpha} f_{\alpha}^{\mathrm{eq}} = \rho \tag{10}$$

$$\sum_{\alpha} f_{\alpha}^{\mathrm{eq}} e_{\alpha} = \rho u \tag{11}$$

$$\sum_{\alpha} f_{\alpha}^{\mathrm{eq}} \varepsilon_{\alpha} = \frac{1}{2}\rho u^2 + \rho E \tag{12}$$

$$\pi^0 \equiv \sum_{\alpha} f_{\alpha}^{\mathrm{eq}} e_{\alpha} e_{\alpha} = \rho u^2 + p \tag{13}$$

$$Q^0 \equiv \sum_{\alpha} f_{\alpha}^{\mathrm{eq}} e_{\alpha} \varepsilon_{\alpha} = \left(\frac{1}{2}\rho u^2 + \rho E + p\right) u \tag{14}$$

$$P^0 \equiv \sum_{\alpha} f_{\alpha}^{\mathrm{eq}} e_{\alpha}^3 = \rho u^3 + 3pu \tag{15}$$

$$R^0 \equiv \sum_{\alpha} f_{\alpha}^{\mathrm{eq}} e_{\alpha}^2 \varepsilon_{\alpha} = \frac{1}{2}\rho u^4 + (2\gamma - 1)\rho E u^2 + \frac{1}{2}(\gamma - 1)\rho u^2 E + (\gamma - 1)\gamma\rho E^2 \tag{16}$$

where p is the pressure of the perfect gas, which is given by

$$p = (\gamma - 1)\rho E \tag{17}$$

Here γ is the specific-heat ratio.

DOI: 10.1002/fld

2.2. *Coefficients in the equilibrium distribution function* f_α^{eq}

Substituting the equilibrium distribution function f_α^{eq} into (10)–(16), we obtain four groups of linear equations for determining the coefficients of f_α^{eq}. They can be expressed as four equations with variable parameters.

The first equation is

$$b(A'_\beta\xi_\beta c_1^4+A''_\beta\eta_\beta c_2^4+B'_\beta\xi_\beta c_1^4+B''_\beta\eta_\beta c_2^4)+\sigma_\beta D_0+\zeta_\beta D_6=z_\beta,\quad \beta=0,2,6,7 \tag{18}$$

Here the parameters are

$$\xi_0=c_1^{-4},\eta_0=c_2^{-4},\sigma_0=1,\zeta_0=0,z_0=1;\quad \xi_2=c_1^{-2},\eta_2=c_2^{-2},\sigma_2=0,\zeta_2=0,z_2=1$$

$$\xi_6=c_1^{-4},\eta_6=c_2^{-4},\sigma_6=0,\zeta_6=1,z_6=0;\quad \xi_7=1,\eta_7=1,\sigma_7=0,\zeta_7=0,z_7=0$$

The second equation is

$$b(A'_\beta\xi_\beta c_1^6+A''_\beta\eta_\beta c_2^6+B'_\beta\xi_\beta c_1^6+B''_\beta\eta_\beta c_2^6)=z_\beta,\quad \beta=0,2,6,7 \tag{19}$$

Here the parameters are

$$\xi_0=c_1^{-4},\eta_0=c_2^{-4},z_0=p/\rho;\quad \xi_2=c_1^{-2},\eta_2=c_2^{-2},z_2=3(\gamma-1)E$$

$$\xi_6=c_1^{-4},\eta_6=c_2^{-4},z_6=1;\quad \xi_7=1,\eta_7=1,z_7=1$$

The third equation is

$$b(A'_\beta\varepsilon_A+A''_\beta\varepsilon_A+B'_\beta\varepsilon_B+B''_\beta\varepsilon_B)+\sigma_\beta D_0\varepsilon_D+\zeta_\beta D_6\varepsilon_D=z_\beta,\quad \beta=0,6 \tag{20}$$

Here the parameters are

$$\sigma_0=1,\zeta_0=0,z_0=E;\quad \sigma_6=0,\zeta_6=1,z_6=\tfrac{1}{2}$$

The fourth equation is

$$b(A'_\beta\varepsilon_A\xi_\beta c_1^4+A''_\beta\varepsilon_A\eta_\beta c_2^4+B'_\beta\varepsilon_B\xi_\beta c_1^4+B''_\beta\varepsilon_B\eta_\beta c_2^4)=z_\beta,\quad \beta=0,2,6,7 \tag{21}$$

Here the parameters are

$$\xi_0=c_1^{-2},\eta_0=c_2^{-2},z_0=\gamma(\gamma-1)E^2;\quad \xi_2=c_1^{-2},\eta_2=c_2^{-2},z_2=\gamma E$$

$$\xi_6=c_1^{-2},\eta_6=c_2^{-2},z_6=\tfrac{1}{2}u^2+\tfrac{1}{2}(5\gamma-3)E;\quad \xi_7=1,\eta_7=1,z_7=\tfrac{1}{2}$$

In order to obtain these coefficients in the equilibrium distribution, we have to propose some man-made complementary conditions. We assume that the particles in type A make the same contribution as the particles in type B for the moments of the equilibrium distribution function. We have the following assumptions, respectively:

$$A'_\beta\varepsilon_A+B'_\beta\varepsilon_B=m_\beta(A''_\beta\varepsilon_A+B''_\beta\varepsilon_B)=z_\beta,\quad \beta=0,2,6,7 \tag{22}$$

DOI: 10.1002/fld

Here the parameters are

$$m_0=4, z_0=\frac{\gamma(\gamma-1)}{2bc^2}E^2; \quad m_2=4, z_2=\frac{\gamma E}{2bc^2}; \quad m_6=4$$

$$z_6=\frac{1}{2bc^2}\left[\frac{1}{2}u^2+\frac{1}{2}(5\gamma-3)E\right]; \quad m_7=16, z_7=\frac{1}{4bc^4}$$

Thus, we obtain

$$A_0'=\frac{1}{\varepsilon_A-\varepsilon_B}\left\{\frac{\gamma(\gamma-1)E^2D}{2bc^2}+\frac{\varepsilon_B pD}{3\rho bc^2}-\frac{4\varepsilon_B}{3b}+\frac{4\varepsilon_B}{3b\varepsilon_D}\left[E-\frac{5\gamma(\gamma-1)E^2D}{8c^2}\right]\right\} \tag{23}$$

$$B_0'=\frac{1}{\varepsilon_A-\varepsilon_B}\left\{-\frac{\gamma(\gamma-1)E^2D}{2bc^2}-\frac{\varepsilon_A pD}{3\rho bc^2}+\frac{4\varepsilon_A}{3b}-\frac{4\varepsilon_A}{3b\varepsilon_D}\left[E-\frac{5\gamma(\gamma-1)E^2D}{8c^2}\right]\right\} \tag{24}$$

$$A_0''=\frac{1}{\varepsilon_A-\varepsilon_B}\left\{\frac{\gamma(\gamma-1)E^2D}{8bc^2}-\frac{\varepsilon_B pD}{3\rho bc^2}+\frac{\varepsilon_B}{3b}-\frac{\varepsilon_B}{3b\varepsilon_D}\left[E-\frac{5\gamma(\gamma-1)E^2D}{8c^2}\right]\right\} \tag{25}$$

$$B_0''=\frac{1}{\varepsilon_A-\varepsilon_B}\left\{-\frac{\gamma(\gamma-1)E^2D}{8bc^2}+\frac{\varepsilon_A pD}{3\rho bc^2}-\frac{\varepsilon_A}{3b}+\frac{\varepsilon_A}{3b\varepsilon_D}\left[E-\frac{5\gamma(\gamma-1)E^2D}{8c^2}\right]\right\} \tag{26}$$

$$D_0=\left[E-\frac{5}{8c^2}\gamma(\gamma-1)E^2\right]\frac{1}{\varepsilon_D} \tag{27}$$

$$A_2'=\frac{1}{\varepsilon_B-\varepsilon_A}\left[\frac{4c^2-3(\gamma-1)E}{3bc^4}\varepsilon_B-\frac{\gamma E}{2bc^2}\right] \tag{28}$$

$$B_2'=\frac{1}{\varepsilon_A-\varepsilon_B}\left[\frac{4c^2-3(\gamma-1)E}{3bc^4}\varepsilon_A-\frac{\gamma E}{2bc^2}\right] \tag{29}$$

$$A_2''=\frac{1}{\varepsilon_B-\varepsilon_A}\left[\frac{3(\gamma-1)E-c^2}{12bc^4}\varepsilon_B-\frac{\gamma E}{8bc^2}\right] \tag{30}$$

$$B_2''=\frac{1}{\varepsilon_A-\varepsilon_B}\left[\frac{3(\gamma-1)E-c^2}{12bc^4}\varepsilon_A-\frac{\gamma E}{8bc^2}\right] \tag{31}$$

$$A_6'=\frac{1}{\varepsilon_B-\varepsilon_A}\left\{-\frac{\varepsilon_B}{3bc^2}-\frac{4\varepsilon_B}{3b\varepsilon_D}\left[\frac{1}{2}-\frac{5}{8c^2}\left(\frac{1}{2}u^2+\frac{5}{2}\gamma E-\frac{3}{2}E\right)\right]-\frac{1}{2bc^2}\left(\frac{1}{2}u^2+\frac{5}{2}\gamma E-\frac{3}{2}E\right)\right\} \tag{32}$$

$$A_6''=\frac{1}{\varepsilon_B-\varepsilon_A}\left\{\frac{\varepsilon_B}{3bc^2}+\frac{\varepsilon_B}{3b\varepsilon_D}\left[\frac{1}{2}-\frac{5}{8c^2}\left(\frac{1}{2}u^2+\frac{5}{2}\gamma E-\frac{3}{2}E\right)\right]-\frac{1}{8bc^2}\left(\frac{1}{2}u^2+\frac{5}{2}\gamma E-\frac{3}{2}E\right)\right\} \tag{33}$$

DOI: 10.1002/fld

$$B_6' = \frac{1}{\varepsilon_A - \varepsilon_B}\left\{-\frac{\varepsilon_A}{3bc^2} - \frac{4\varepsilon_A}{3b\varepsilon_D}\left[\frac{1}{2} - \frac{5}{8c^2}\left(\frac{1}{2}u^2 + \frac{5}{2}\gamma E - \frac{3}{2}E\right)\right] - \frac{1}{2bc^2}\left(\frac{1}{2}u^2 + \frac{5}{2}\gamma E - \frac{3}{2}E\right)\right\} \tag{34}$$

$$B_6'' = \frac{1}{\varepsilon_A - \varepsilon_B}\left\{\frac{\varepsilon_A}{3bc^2} + \frac{\varepsilon_A}{3b\varepsilon_D}\left[\frac{1}{2} - \frac{5}{8c^2}\left(\frac{1}{2}u^2 + \frac{5}{2}\gamma E - \frac{3}{2}E\right)\right] - \frac{1}{8bc^2}\left(\frac{1}{2}u^2 + \frac{5}{2}\gamma E - \frac{3}{2}E\right)\right\} \tag{35}$$

$$D_6 = \frac{1}{\varepsilon_D}\left\{\frac{1}{2} - \frac{5}{8c^2}\left[\frac{1}{2}u^2 + \frac{1}{2}(5\gamma - 3)E\right]\right\} \tag{36}$$

$$A_7' = \frac{1}{\varepsilon_B - \varepsilon_A}\left(-\frac{\varepsilon_B}{3bc^6} - \frac{1}{4bc^4}\right) \tag{37}$$

$$B_7' = \frac{1}{\varepsilon_A - \varepsilon_B}\left(-\frac{\varepsilon_A}{3bc^6} - \frac{1}{4bc^4}\right) \tag{38}$$

$$A_7'' = \frac{1}{\varepsilon_B - \varepsilon_A}\left(\frac{\varepsilon_B}{48bc^6} - \frac{1}{64bc^4}\right) \tag{39}$$

$$B_7'' = \frac{1}{\varepsilon_A - \varepsilon_B}\left(\frac{\varepsilon_A}{48bc^6} - \frac{1}{64bc^4}\right) \tag{40}$$

3. GHOST FIELD DISTRIBUTION AND THE EULER EQUATIONS

3.1. Higher-order moments of the ghost field distribution functions

According to Equations (7)–(12), the ghost field distribution g_α has the following feature [36]:

$$\sum_\alpha g_\alpha^{\mathrm{eq}} = 0 \tag{41}$$

$$\sum_\alpha g_\alpha^{\mathrm{eq}} e_\alpha = 0 \tag{42}$$

$$\sum_\alpha g_\alpha^{\mathrm{eq}} \varepsilon_\alpha = 0 \tag{43}$$

The meaning is that the macroscopic mass, momentum and energy of the ghost field distribution g_α are zero. We also assume that its momentum-flux and energy-flux are zero, say,

$$\sum_\alpha g_\alpha^{\mathrm{eq}} e_\alpha e_\alpha = 0 \tag{44}$$

$$\sum_\alpha g_\alpha^{\mathrm{eq}} e_\alpha \varepsilon_\alpha = 0 \tag{45}$$

DOI: 10.1002/fld

In order to remove the nonphysical viscosity, we design the higher-order moments of the ghost field distribution g_α as

$$\sum_\alpha g_\alpha^{\mathrm{eq}} e_\alpha^3 = P' \tag{46}$$

$$\sum_\alpha g_\alpha^{\mathrm{eq}} e_\alpha^2 \varepsilon_\alpha = R' \tag{47}$$

where functions P' and R' are determined by the viscous term according to the macroscopic equation. In Equations (41)–(47), these higher-order moments are zero except $\sum_\alpha g_\alpha^{\mathrm{eq}} e_\alpha^3 = P' \neq 0$ and $\sum_\alpha g_\alpha^{\mathrm{eq}} e_\alpha^2 \varepsilon_\alpha = R' \neq 0$; therefore, g_α is named as ghost field distribution.

We assume that the ghost field equilibrium distribution function g_α^{eq} has the following form:

$$g_\alpha^{\mathrm{eq}} = a_0'\rho + a_2'\rho u e_\alpha + a_6'\rho u^2 + a_7'\rho u^3 e_\alpha^3 \quad (\alpha = 1,2), \quad \varepsilon_\alpha = \varepsilon_A$$

$$g_\alpha^{\mathrm{eq}} = a_0''\rho + a_2''\rho u e_\alpha + a_6''\rho u^2 + a_7''\rho u^3 e_\alpha^3 \quad (\alpha = 3,4), \quad \varepsilon_\alpha = \varepsilon_A$$

$$g_\alpha^{\mathrm{eq}} = b_0'\rho + b_2'\rho u e_\alpha + b_6'\rho u^2 + b_7'\rho u^3 e_\alpha^3 \quad (\alpha = 5,6), \quad \varepsilon_\alpha = \varepsilon_B$$

$$g_\alpha^{\mathrm{eq}} = b_0''\rho + b_2''\rho u e_\alpha + b_6''\rho u^2 + b_7''\rho u^3 e_\alpha^3 \quad (\alpha = 7,8), \quad \varepsilon_\alpha = \varepsilon_B$$

$$g_0^{\mathrm{eq}} = d_0\rho + d_6\rho u^2 \quad (\alpha = 0), \quad \varepsilon_\alpha = \varepsilon_D$$

where coefficients $a_\beta', a_\beta'', b_\beta', b_\beta''$ and d_β are determined by Equations (41)–(47) and a set of reasonable man-made conditions.

3.2. Coefficients in the equilibrium distribution of the ghost field

Substituting the equilibrium distribution function g_α^{eq} into (41)–(47), we obtain four groups of linear equations for determining the coefficients of g_α^{eq}. They can be expressed as four equations with variable parameters.

The first equation is

$$b(a_\beta'\xi_\beta c_1^4 + a_\beta''\eta_\beta c_2^4 + b_\beta'\xi_\beta c_1^4 + b_\beta''\eta_\beta c_2^4) + \sigma_\beta d_0 + \zeta_\beta d_6 = 0, \quad \beta = 0,2,6,7 \tag{48}$$

Here the parameters are

$$\xi_0 = c_1^{-4}, \eta_0 = c_2^{-4}, \sigma_0 = 1, \zeta_0 = 0; \quad \xi_2 = c_1^{-2}, \eta_2 = c_2^{-2}, \sigma_2 = 0, \zeta_2 = 0$$

$$\xi_6 = c_1^{-4}, \eta_6 = c_2^{-4}, \sigma_6 = 0, \zeta_6 = 1; \quad \xi_7 = 1, \eta_7 = 1, \sigma_7 = 0, \zeta_7 = 0$$

The second equation is

$$b(a_\beta'\varepsilon_A + a_\beta''\varepsilon_A + b_\beta'\varepsilon_B + b_\beta''\varepsilon_B) + d_\beta\varepsilon_D = 0, \quad \beta = 0,6 \tag{49}$$

The third equation is

$$a_\beta'\xi_\beta c_1^4 + a_\beta''\eta_\beta c_2^4 + b_\beta'\sigma_\beta c_1^4 + b_\beta''\zeta_\beta c_2^4 = 0, \quad \beta = 0,2,6,7 \tag{50}$$

DOI: 10.1002/fld

Here the parameters are

$$\xi_0=c_1^{-2},\eta_0=c_2^{-2},\sigma_0=c_1^{-2},\zeta_0=c_2^{-2};\quad \xi_2=c_1^{-2}\varepsilon_A,\eta_2=c_2^{-2}\varepsilon_A,\sigma_2=c_1^{-2}\varepsilon_B,\zeta_2=c_2^{-2}\varepsilon_B$$

$$\xi_6=c_1^{-2},\eta_6=c_2^{-2},\sigma_6=c_1^{-2},\zeta_6=c_2^{-2};\quad \xi_7=\varepsilon_A,\eta_7=\varepsilon_A,\sigma_7=\varepsilon_B,\zeta_7=\varepsilon_B$$

The fourth equation is

$$\begin{aligned}\rho ub(a_2'c_1^4+a_2''c_2^4+b_2'c_1^4+b_2''c_2^4)+\rho u^3b(a_7'c_1^6+a_7''c_2^6+b_7'c_1^6+b_7''c_2^6)&=P'\\ b\rho(a_0'\varepsilon_Ac_1^2+a_0''\varepsilon_Ac_2^2+b_0'\varepsilon_Bc_1^2+b_0''\varepsilon_Bc_2^2)+\rho u^2b(a_6'\varepsilon_Ac_1^2+a_6''\varepsilon_Ac_2^2+b_6'\varepsilon_Bc_1^2+b_6''\varepsilon_Bc_2^2)&=R'\end{aligned}\tag{51}$$

In order to obtain these coefficients in the equilibrium distribution g_α^{eq}, we have to propose some artificial complementary conditions. We assume that the particles in type A make the same contribution as the particles in type B for the moments of the ghost field equilibrium distribution function. We have the following assumptions:

$$a_\beta'\varepsilon_A+b_\beta'\varepsilon_B=m_\beta(a_\beta''\varepsilon_A+b_\beta''\varepsilon_B),\quad \beta=0,2,6,7,\quad m_0=4,\quad m_2=4,\quad m_6=4,\quad m_7=16\tag{52}$$

and

$$a_\beta'+b_\beta'=n_\beta(a_\beta''+b_\beta''),\quad \beta=6,7,\quad n_6=4,\quad n_7=16\tag{53}$$

Thus, we have

$$a_0'=\frac{1}{\varepsilon_B-\varepsilon_A}\frac{R'}{2\rho bc^2}\left(\frac{5\varepsilon_B}{3\varepsilon_D}-1\right)\tag{54}$$

$$b_0'=\frac{1}{\varepsilon_A-\varepsilon_B}\frac{R'}{2\rho bc^2}\left(\frac{5\varepsilon_A}{3\varepsilon_D}-1\right)\tag{55}$$

$$a_0''=-\frac{1}{\varepsilon_B-\varepsilon_A}\frac{R'}{8\rho bc^2}\left(\frac{5\varepsilon_B}{3\varepsilon_D}+1\right)\tag{56}$$

$$b_0''=-\frac{1}{\varepsilon_A-\varepsilon_B}\frac{R'}{8\rho bc^2}\left(\frac{5\varepsilon_A}{3\varepsilon_D}+1\right)\tag{57}$$

$$d_0=-\frac{5R'}{8\rho c^2\varepsilon_D}\tag{58}$$

$$a_2'=-\frac{1}{\varepsilon_B-\varepsilon_A}\frac{P'\varepsilon_B}{3\rho ubc^4}\tag{59}$$

$$b_2'=-\frac{1}{\varepsilon_A-\varepsilon_B}\frac{P'\varepsilon_A}{3\rho ubc^4}\tag{60}$$

$$a_2''=\frac{1}{\varepsilon_B-\varepsilon_A}\frac{P'\varepsilon_B}{12\rho ubc^4}\tag{61}$$

$$b_2''=\frac{1}{\varepsilon_A-\varepsilon_B}\frac{P'\varepsilon_A}{12\rho ubc^4}\tag{62}$$

DOI: 10.1002/fld

$$a_6' = b_6' = a_6'' = b_6'' = 0 \tag{63}$$

$$d_6 = 0 \tag{64}$$

$$a_7' = b_7' = a_7'' = b_7'' = 0 \tag{65}$$

3.3. One-dimensional Euler equations with second-order accuracy

Using a small parameter k as the time step in numerical simulation, we take it equal to the Knudsen number [6]. The lattice Boltzmann equation in physical unit is

$$F_\alpha(\mathbf{x}+ke_\alpha, t+k) - F_\alpha(\mathbf{x}, t) = -\frac{1}{\tau}(F_\alpha(\mathbf{x}, t) - F_\alpha^{\mathrm{eq}}(\mathbf{x}, t)) \tag{66}$$

The Chapman–Enskog expansion [37] is applied to $F_\alpha(\mathbf{x}, t)$ under the assumption of the small Knudsen number k,

$$F_\alpha = \sum_{n=0}^{\infty} k^n F_\alpha^n = F_\alpha^0 + kF_\alpha^1 + k^2 F_\alpha^2 + \cdots \tag{67}$$

In Equation (67) F_α^0 is F_α^{eq}. We discuss the changes in different time scales, introduced as $t_0, t_1, \ldots$; thus,

$$t_0 = t, \quad t_1 = kt, \quad t_2 = k^2 t, \quad t_3 = k^3 t \ldots$$

and

$$\frac{\partial}{\partial t} = \frac{\partial}{\partial t_0} + k\frac{\partial}{\partial t_1} + k^2\frac{\partial}{\partial t_2} + k^3\frac{\partial}{\partial t_3} + k^4\frac{\partial}{\partial t_4} + O(k^5) \tag{68}$$

Performing the Taylor expansion upon Equation (66), and retaining terms up to $O(k^5)$, we obtain a series of lattice Boltzmann equations in different time t_0, t_1, t_2 scales [6]:

$$\frac{\partial F_\alpha^{\mathrm{eq}}}{\partial t_0} + e_\alpha\frac{\partial F_\alpha^{\mathrm{eq}}}{\partial x} = -\frac{1}{\tau}F_\alpha^1 \tag{69}$$

$$\frac{\partial F_\alpha^{\mathrm{eq}}}{\partial t_1} + \left(\frac{1}{2}-\tau\right)\left(\frac{\partial}{\partial t_0} + e_\alpha\frac{\partial}{\partial x}\right)^2 F_\alpha^{\mathrm{eq}} = -\frac{1}{\tau}F_\alpha^2 \tag{70}$$

$$\frac{\partial F_\alpha^{\mathrm{eq}}}{\partial t_2} + (1-2\tau)\left(\frac{\partial}{\partial t_0} + e_\alpha\frac{\partial}{\partial x}\right)\frac{\partial F_\alpha^{\mathrm{eq}}}{\partial t_1} + \left(\tau^2-\tau+\frac{1}{6}\right)\left(\frac{\partial}{\partial t_0} + e_\alpha\frac{\partial}{\partial x}\right)^3 F_\alpha^{\mathrm{eq}} = -\frac{1}{\tau}F_\alpha^3 \tag{71}$$

$$\begin{aligned}&\frac{\partial F_\alpha^{\mathrm{eq}}}{\partial t_3} + \left(\frac{1}{2}-\tau\right)\frac{\partial^2}{\partial t_1^2}F_\alpha^{\mathrm{eq}} + 2\left(\frac{1}{2}-\tau\right)\left(\frac{\partial}{\partial t_0} + e_\alpha\frac{\partial}{\partial x}\right)\frac{\partial}{\partial t_2}F_\alpha^{\mathrm{eq}}\\ &\quad + 3\left(\tau^2-\tau+\frac{1}{6}\right)\left(\frac{\partial}{\partial t_0} + e_\alpha\frac{\partial}{\partial x}\right)^2\frac{\partial}{\partial t_1}F_\alpha^{\mathrm{eq}}\\ &\quad + \left(-\tau^3+\frac{3}{2}\tau^2-\frac{7}{12}\tau+\frac{1}{24}\right)\left(\frac{\partial}{\partial t_0} + e_\alpha\frac{\partial}{\partial x}\right)^4 F_\alpha^{\mathrm{eq}} = -\frac{1}{\tau}F_\alpha^4\end{aligned} \tag{72}$$

DOI: 10.1002/fld

To derive the equations for ρ, ρu and $\frac{1}{2}\rho u^2+\rho E$ to first order in k, a summation of Equation (69) with respect to α is taken to give the first-order macroscopic equations. This equation is named as the conservation laws in the first time scale t_0,

$$\frac{\partial \rho}{\partial t_0}+\frac{\partial \rho u}{\partial x}=0 \tag{73}$$

$$\frac{\partial \rho u}{\partial t_0}+\frac{\partial \pi^0}{\partial x}=0 \tag{74}$$

$$\frac{\partial(\frac{1}{2}\rho u^2+\rho E)}{\partial t_0}+\frac{\partial Q^0}{\partial x}=0 \tag{75}$$

The second-order macroscopic equations are obtained by taking $(69)+(70)\times k$ and summation over α. Thus, we have

$$\frac{\partial \rho}{\partial t}+\frac{\partial \rho u}{\partial x}=O(k^2) \tag{76}$$

$$\frac{\partial \rho u}{\partial t}+\frac{\partial \pi^0}{\partial x}=k\left(\tau-\frac{1}{2}\right)\frac{\partial}{\partial x}\left[\frac{\partial P'}{\partial x}+(\gamma-1)(3-\gamma)\rho E\frac{\partial u}{\partial x}\right]+O(k^2) \tag{77}$$

$$\frac{\partial\left(\frac{1}{2}\rho u^2+\rho E\right)}{\partial t}+\frac{\partial Q^0}{\partial x}=k\left(\tau-\frac{1}{2}\right)\frac{\partial}{\partial x}\left[\frac{\partial R'}{\partial x}+(\gamma-1)(3-\gamma)\rho E u\frac{\partial u}{\partial x}+\gamma(\gamma-1)\rho E\frac{\partial E}{\partial x}\right]+O(k^2) \tag{78}$$

when functions P' and R' satisfy the following conditions:

$$\frac{\partial P'}{\partial x}=-(\gamma-1)(3-\gamma)\rho E\frac{\partial u}{\partial x} \tag{79}$$

$$\frac{\partial R'}{\partial x}=-(\gamma-1)(3-\gamma)\rho E u\frac{\partial u}{\partial x}-\gamma(\gamma-1)\rho E\frac{\partial E}{\partial x} \tag{80}$$

The Euler equations with second-order accuracy are obtained as

$$\frac{\partial \rho}{\partial t}+\frac{\partial \rho u}{\partial x}=O(k^2) \tag{81}$$

$$\frac{\partial \rho u}{\partial t}+\frac{\partial(\rho u^2+p)}{\partial x}=O(k^2) \tag{82}$$

$$\frac{\partial(\frac{1}{2}\rho u^2+\rho E)}{\partial t}+\frac{\partial(\frac{1}{2}\rho u^3+\gamma\rho E u)}{\partial x}=O(k^2) \tag{83}$$

DOI: 10.1002/fld

In Equations (81)–(83), we can use the finite difference method to find the numerical solutions of P' and R'. The first-order difference schemes are

$$P'_{j+1} = P'_j + \Delta x \frac{\partial P'_j}{\partial x} \tag{84}$$

$$R'_{j+1} = R'_j + \Delta x \frac{\partial R'_j}{\partial x} \tag{85}$$

The second-order difference schemes are

$$P'_{j+1} = P'_j + \Delta x \frac{\partial P'_j}{\partial x} + \frac{1}{2}\Delta x^2 \frac{\partial^2 P'_j}{\partial x^2} \tag{86}$$

$$R'_{j+1} = R'_j + \Delta x \frac{\partial R'_j}{\partial x} + \frac{1}{2}\Delta x^2 \frac{\partial^2 R'_j}{\partial x^2} \tag{87}$$

4. NUMERICAL EXAMPLES

In this section four famous test problems [17] are simulated to examine the performance of this model.

4.1. The Sod problem

In the Sod problem, the initial condition (at $t = 0.0$) is defined by

$$\begin{aligned} (\rho, u, p) &= (1.0, 0.0, 1.0) \quad \text{if } 0.0 \leqslant x \leqslant 0.5 \\ (\rho, u, p) &= (0.125, 0.0, 0.1) \quad \text{if } 0.5 < x \leqslant 1.0 \end{aligned} \tag{88}$$

The results of the density ρ, pressure p, velocity u and the internal energy E calculated by using the LBM at the time $t = 100\Delta t$ are plotted in Figures 2 and 3. In this numerical experiment, the time step is $\Delta t = \Delta x/c = 1.667 \times 10^{-3}$. The boundary conditions at the two ends are Dirichlet conditions. The internal energy E is calculated by $E = p/\rho(\gamma - 1)$. In addition, the variables P' and R' are computed by using the first-order difference scheme (84)–(85) in Figure 2 and the second-order difference scheme (86)–(87) in Figure 3. In these two figures, the same values for parameters are selected.

By comparing these results with the exact solutions, we find the shock waves and the contact discontinuities are spread over typically three to four grid cells in Figure 2 and two to three grid cells in Figure 3. The two figures show that the method with first-order scheme has slightly higher resolution than the LBM method in Reference [28] and the result from the second-order scheme in Figure 3 is higher in resolution than that from the first-order scheme in Figure 2.

We also plot the curves of the infinite norm of the relative error $\|\mathrm{Er}\|_\infty = \max_{1 \leqslant j \leqslant m} |(u^{\mathrm{N}} - u^{\mathrm{E}})/u^{\mathrm{E}}|$ versus the Knudsen number k for the example (u^{N} is the numerical result by lattice Boltzmann model, and u^{E} is the exact solution); see Figure 4. This figure shows the relations between $\|\mathrm{Er}\|_\infty$ and the Knudsen number k. We find that the result of the second-order difference

DOI: 10.1002/fld

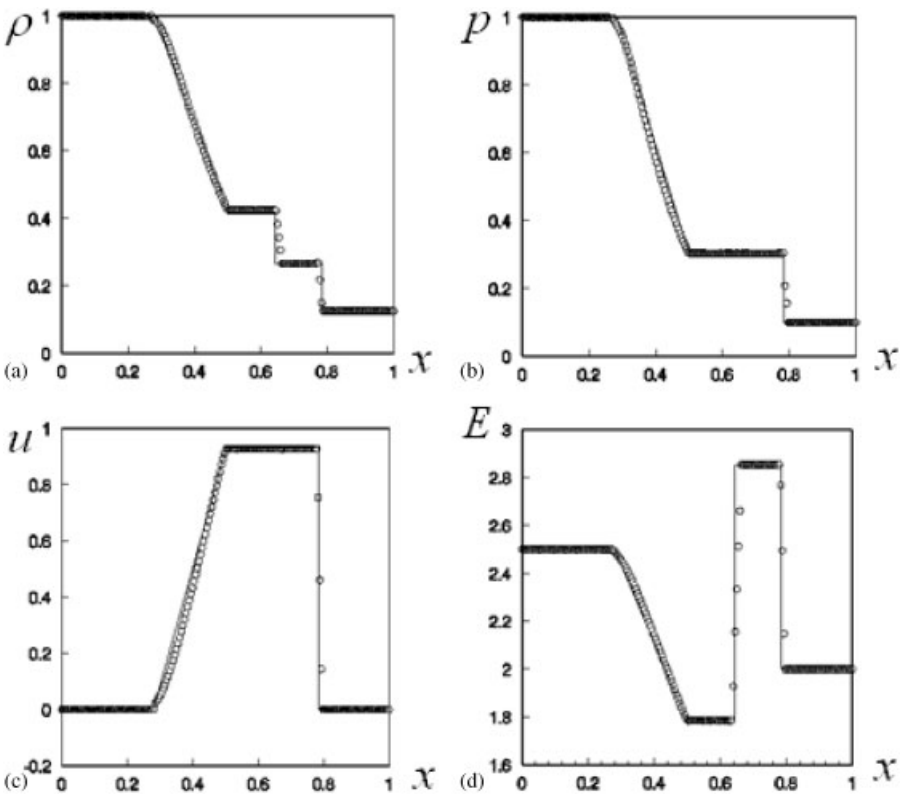

Figure 2. Comparison of the exact solution and the LBM results of one-dimensional Sod problem. Solid lines are exact solutions, and circles are LBM results: (a) density; (b) pressure; (c) velocity; and (d) internal energy. The parameters are $\gamma=1.4, c=3.0, \tau=1.51, \varepsilon_A=2c^2, \varepsilon_B=0.6c^2, \varepsilon_D=0.13c^2$, lattice size$=200$ and time $t=100\Delta t$. The variables P' and R' are computed by using the first-order difference schemes (84)–(85).

schemes for P' and R' is better than the first-order method. This figure provides some qualitative trends for the numerical order of convergence.

4.2. *The Lax problem*

The initial condition (at $t=0.0$) for Lax problem is

$$\begin{aligned}(\rho, u, p) &= (0.445, 0.698, 3.528) \quad \text{if } 0.0 \leqslant x \leqslant 0.5 \\ (\rho, u, p) &= (0.5, 0.0, 0.571) \quad \text{if } 0.5 < x \leqslant 1.0\end{aligned} \tag{89}$$

In the numerical experiments for Lax problem, the time step is also $\Delta t=\Delta x/c=1.667\times10^{-3}$. The boundary conditions at the two ends of the domain are Dirichlet conditions. The results of LBM and exact solutions are shown as the density ρ, pressure p, velocity u and the internal energy E at the time $t=100\Delta t$ in Figures 5 and 6. The internal energy E is calculated by $E=p/\rho(\gamma-1)$. In Figure 5, the difference scheme for the variables P' and R' is the first order and expressed

DOI: 10.1002/fld

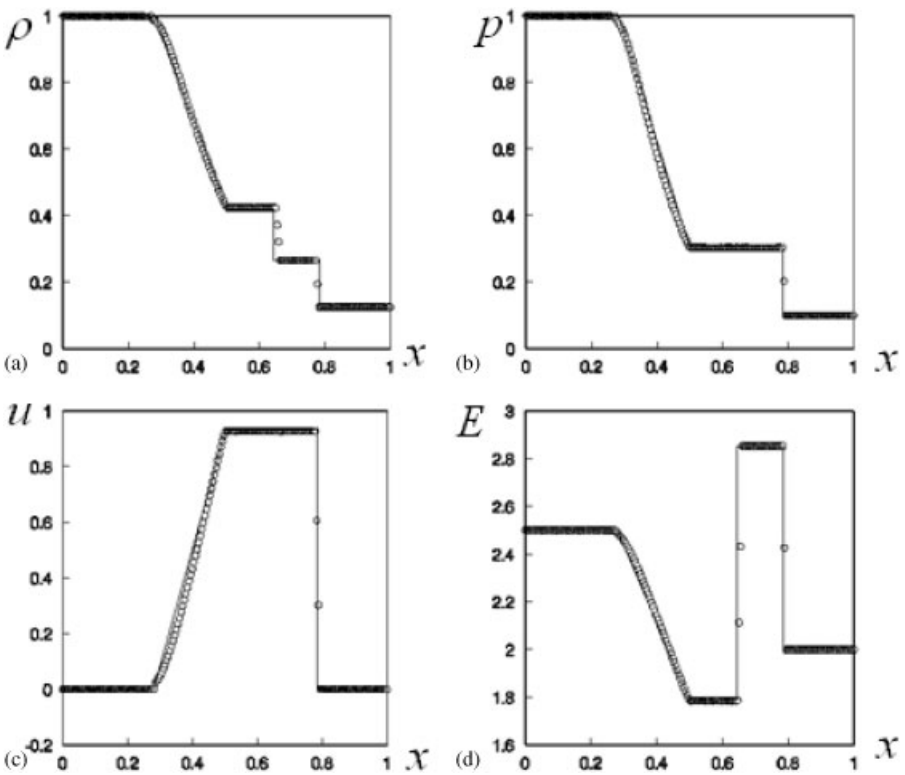

Figure 3. Comparison of the exact solution and the LBM results of one-dimensional Sod problem. Solid lines are exact solutions, and circles are LBM results: (a) density; (b) pressure; (c) velocity; and (d) internal energy. The parameters are $\gamma=1.4, c=3.0, \tau=1.51, \varepsilon_A=2c^2, \varepsilon_B=0.6c^2, \varepsilon_D=0.13c^2$. The lattice size is 200, and time $t=100\Delta t$. The variables P' and R' are computed by using second-order difference schemes (86)–(87).

as (84)–(85), and Figure 6 shows the results from the second-order difference scheme for P' and R' (86)–(87). In these two figures, the solid lines are the exact solutions, and circles are LBM results: (a) density; (b) pressure; (c) velocity; and (d) internal energy. The parameters are $\gamma=1.4$, $c=3.0$, $\tau=1.51$, $\varepsilon_A=2c^2$, $\varepsilon_B=0.6c^2$, $\varepsilon_D=0.13c^2$ and the lattice size is 200.

In Figure 6, we can see the shock waves and the contact discontinuities are spread over typically two to three grid cells. By comparing with the results in Figure 5, this simulation with the second-order difference scheme for the variables P' and R' is of slightly higher accuracy and resolution than that with the first-order difference scheme for P' and R'.

4.3. The Roe problem, case I

The initial condition (at $t=0.0$) for Roe problem is defined as

$$\begin{aligned}(\rho, u, p) &= (1.0, -1.0, 1.8) \quad \text{if } 0.0 \leqslant x \leqslant 0.5\\ (\rho, u, p) &= (1.0, 1.0, 1.8) \quad \text{if } 0.5 < x \leqslant 1.0\end{aligned} \tag{90}$$

DOI: 10.1002/fld

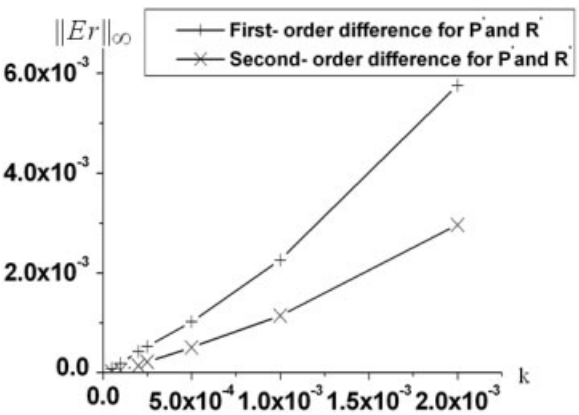

Figure 4. The curves of the infinite norm of the relative error $\mathrm{Er}=|(u^{\mathrm{N}}-u^{\mathrm{E}})/u^{\mathrm{E}}|$ versus the Knudsen number k to example 1. The parameters are $\gamma=1.4$, $c=3.0$, $\tau=1.51$, $\varepsilon_A=2c^2$, $\varepsilon_B=0.6c^2$, $\varepsilon_D=0.13c^2$ and the lattice size is 200.

The results for Roe problem of case I is shown as the form of the density ρ, pressure p, velocity u and the internal energy E at the time $t=100\Delta t$ in Figures 7 and 8. Our numerical experiments show that for Roe problem the time step is $\Delta t=\Delta x/c=1.667\times10^{-3}$. Dirichlet boundary conditions are adopted at the two ends. The expression for the internal energy E is $E=p/\rho(\gamma-1)$, too. Figures 7 and 8 display the results from the first- and second-order difference schemes for P' and R' separately. In the two figures, the solid lines are exact solutions, and circles are LBM results: (a) density; (b) pressure; (c) velocity; and (d) internal energy. The parameters are $\gamma=1.4$, $c=3.0$, $\tau=1.35$, $\varepsilon_A=2c^2$, $\varepsilon_B=0.6c^2$, $\varepsilon_D=0.1c^2$. The lattice size is 200.

The result in Figure 7 is better than the result found in Reference [17]. The simulation with second-order difference scheme for the variables P' and R' in Figure 8 is slightly higher in accuracy and resolution than the first-order difference scheme results.

4.4. The Roe problem, case II

The initial condition (at $t=0.0$) for the problem is

$$\begin{aligned}(\rho, u, p) &= (1.0, -2.0, 0.4) \quad \text{if } 0.0\leqslant x\leqslant 0.5\\ (\rho, u, p) &= (1.0, 2.0, 0.4) \quad \text{if } 0.5< x\leqslant 1.0\end{aligned} \tag{91}$$

The numerical simulation is limited to a near-vacuum case, namely, the near-vacuum region contains the flow. It is known that the density and pressure always take a positive value. An available technique is, for this case, to assume a limit on the relaxation factor, when the density $\rho/\rho_0<\widetilde{k}$, then the collision vanishes, where ρ_0 is the characteristic density, and $\widetilde{k}$ is a limit of the ratio of ρ to ρ_0 [38].

In this model, the mean free path l is equal to $c\cdot k$. We assume that the gas is near-vacuum if collision does not occur in the range of l. However, if we delay the time, i.e. increase the collision time, collisions will surely occur. Therefore, we define the vacuum as a region where there are no

DOI: 10.1002/fld

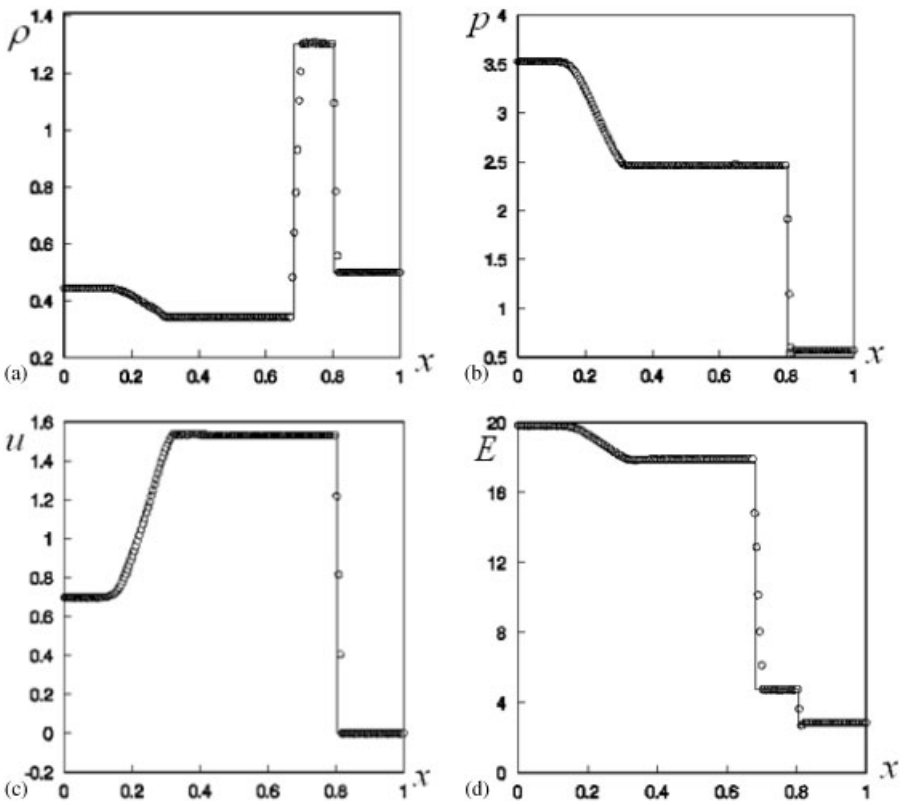

Figure 5. Comparison of the exact solution and the LBM results of one-dimensional Lax problem. Solid lines are exact solutions, and Circles are LBM results: (a) density; (b) pressure; (c) velocity; and (d) internal energy. The parameters are $\gamma=1.4, c=3.0, \tau=1.51, \varepsilon_A=2c^2, \varepsilon_B=0.6c^2, \varepsilon_D=0.13c^2$. The lattice size is 200, and time $t=100\Delta t$. The variables P' and R' are computed by using first-order difference schemes (84)–(85).

particle collisions in the interval of t to $t+\Delta t$, Thus, the limitation of the relaxation factor may be expressed as

$$\widetilde{\tau}=\begin{cases}\tau, & \dfrac{\rho}{\rho_0}<\widetilde{k}\\ \infty, & \dfrac{\rho}{\rho_0}>\widetilde{k}\end{cases} \tag{92}$$

The results of the density ρ and pressure p calculated by using LBM at the time $t=50\Delta t$ are shown in Figure 9(a) and (b), respectively. For this problem, the time step is $\Delta t=\Delta x/c=1.667\times10^{-3}$. The boundary conditions are Dirichlet conditions. The internal energy E is calculated by $E=p/\rho(\gamma-1)$. The variables P' and R' are computed by using first-order difference schemes (84)–(85). In this figure, the parameters are $\gamma=1.4, c=3.0, \tau=1.31, \varepsilon_A=6.5c^2, \varepsilon_B=2.0c^2, \varepsilon_D=0.02c^2, \widetilde{k}=k$, and the lattice size is 200. This method is of slightly higher resolution than the LBM method in Reference [28].

DOI: 10.1002/fld

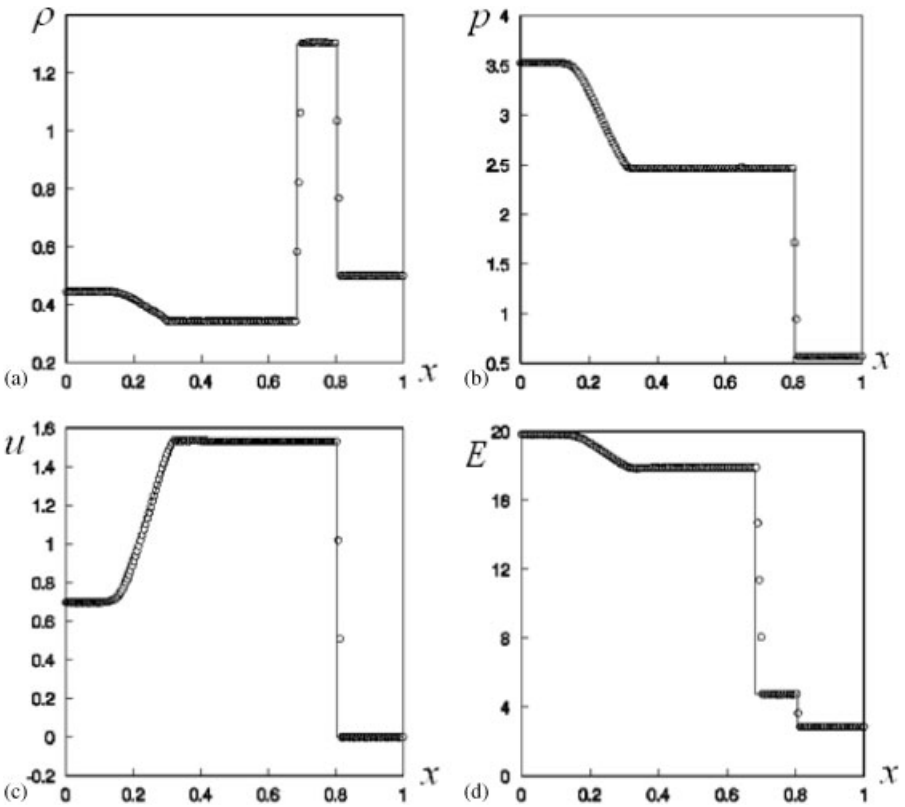

Figure 6. Comparison of the exact solution and the LBM results of one-dimensional Lax problem. Solid lines are exact solutions, and circles are LBM results: (a) density; (b) pressure; (c) velocity; and (d) internal energy. The parameters are $\gamma = 1.4, c = 3.0, \tau = 1.51, \varepsilon_A = 2c^2, \varepsilon_B = 0.6c^2, \varepsilon_D = 0.13c^2$. The lattice size is 200, and time $t = 100\Delta t$. The variables P' and R' are computed by using second-order difference schemes (86)–(87).

Figure 10(a) and (b) shows the results of the density ρ and pressure p calculated by using LBM at the time $t = 50\Delta t$ with the second-order difference scheme for the variables P' and R' (86)–(87). The parameters are the same as those in Figure 9 except $\widetilde{k} = 0.1k$. The simulation with second-order difference scheme for the variables P' and R' has slightly higher accuracy and resolution than the first-order difference scheme ones.

4.5. The comparisons between the first-order model and the second-order model

In this paper, we proposed an LBM for the second-order compressible Euler equations. In comparison with the first-order model in Reference [28], it has higher accuracy and better resolution. From Figures 2–5, we found that (1) the widths of the shock waves are about three to four cells when using the first-order difference scheme (84)–(85), and two to three cells when using the second-order difference scheme (86)–(87). (2) The errors at the contact discontinuities appearing in the first-order model have been eliminated. (3) The non-physical oscillation in the front of the

DOI: 10.1002/fld

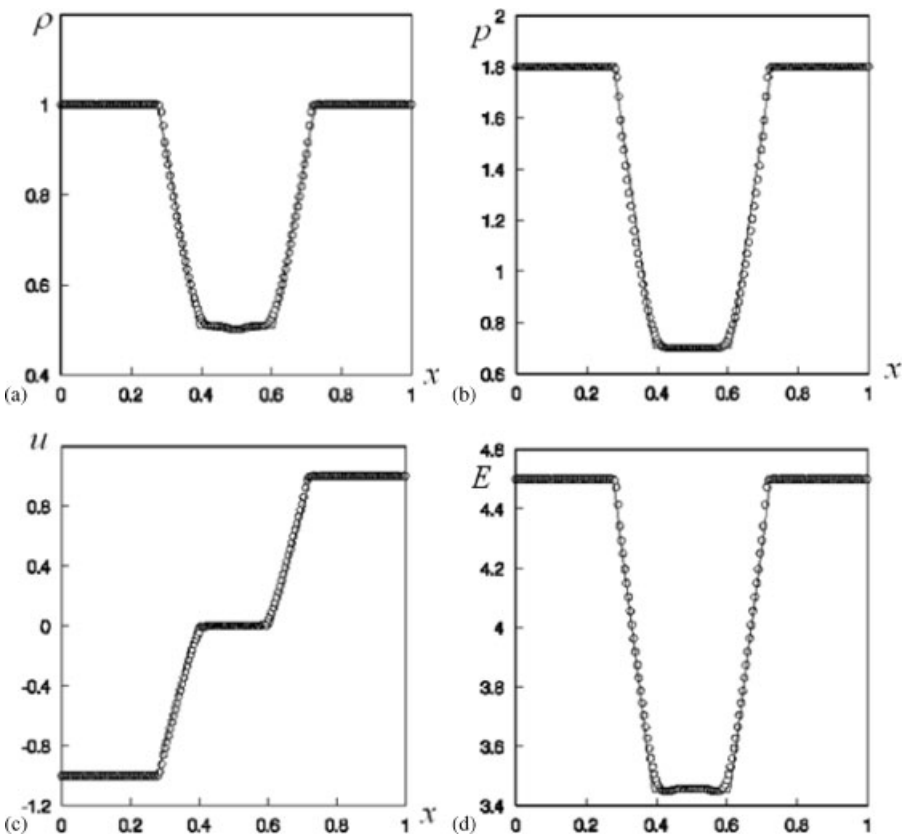

Figure 7. Comparison of the exact solution and the LBM results of one-dimensional Roe problem. Solid lines are exact solutions, and circles are LBM results: (a) density; (b) pressure; (c) velocity; and (d) internal energy. The parameters are $\gamma = 1.4, c = 3.0, \tau = 1.35, \varepsilon_A = 2c^2, \varepsilon_B = 0.6c^2, \varepsilon_D = 0.13c^2$. The lattice size is 200, and time $t = 100\Delta t$. The variables P' and R' are computed by using first-order difference schemes (84)–(85).

shock wave has been weakened. The viscous term is a non-physical term and a positive numerical viscous term. It can weaken the oscillation in the front of the shock wave. This non-physical term is the crux of the matter for the second-order Euler equations. In other words, by comparison of the current results with those in Reference [30], the improvement of the numerical results is obvious. Table I shows the L_1 norm errors in our lattice Boltzmann model and other schemes.

In Table I, a detailed comparison between the lattice Boltzmann schemes and the traditional difference scheme is given. These traditional schemes contain [39]

1. The first-order Lax–Friedrichs scheme (LxF).
2. The ordinary non-staggered non-oscillatory central difference scheme (ORD).
3. The Harten's second-order accuracy upwind scheme (ULT1).
4. The Harten's second-order accuracy upwind with artificial compressible second-order added to ULT1, named as ULTC.

DOI: 10.1002/fld

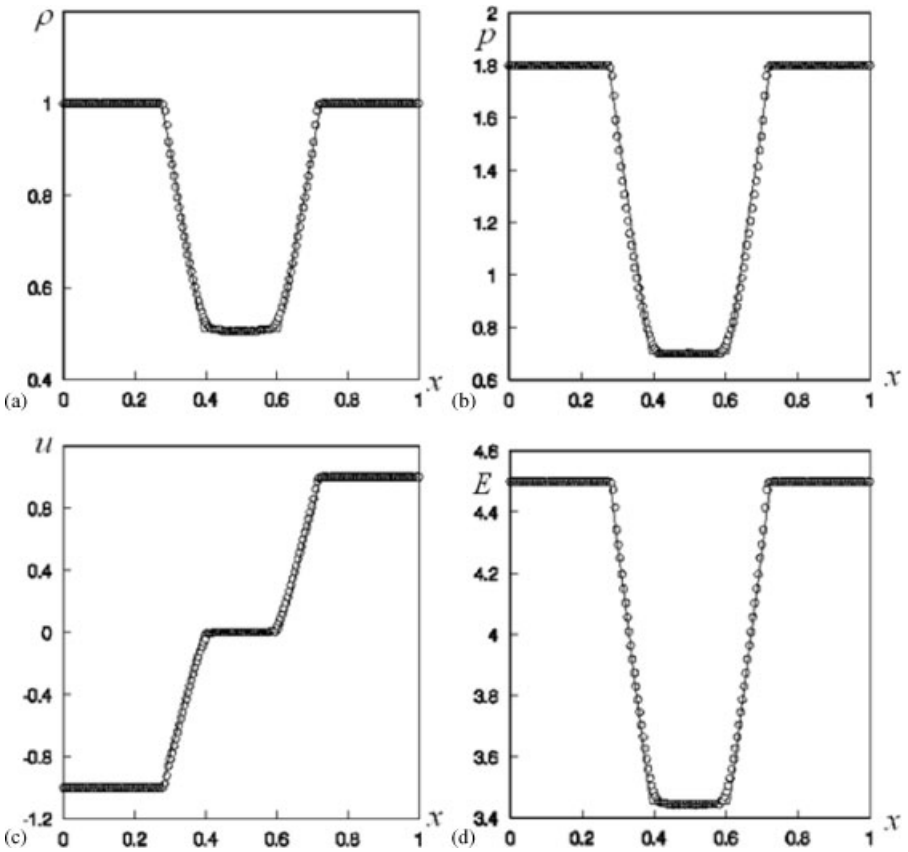

Figure 8. Comparison of the exact solution and the LBM results of one-dimensional Roe problem. Solid lines are exact solutions, and circles are LBM results: (a) density; (b) pressure; (c) velocity; and (d) internal energy. The parameters are $\gamma = 1.4, c = 3.0, \tau = 1.35, \varepsilon_A = 2c^2, \varepsilon_B = 0.6c^2, \varepsilon_D = 0.1c^2$. The lattice size is 200, and time $t = 100\Delta t$. The variables P' and R' are computed by using second-order difference schemes (86)–(87).

5. The second-order staggered non-oscillatory central difference scheme (STG).
6. The STG scheme with a limiter value. This scheme is referred to as STG2.
7. The STG scheme with the component-wise unify non-oscillatory scheme. This scheme is referred to as STGU.
8. The STG scheme with the artificial compression method. This scheme is referred to as STGC.
9. The upwind Godunov scheme is referred to as ROE.

We simulated the Sod and the Lax problems by using the lattice Boltzmann model. Two difference schemes are used for the variables P' and R'. We observe that our LBM schemes, first-order difference schemes (84)–(85) and second-order difference scheme (86)–(87) P' and R', the first-order scheme and LBM in Reference [30] is similar, though the discontinuity is more than two to three cells. However, the second-order scheme possesses more resolution and accuracy and

DOI: 10.1002/fld

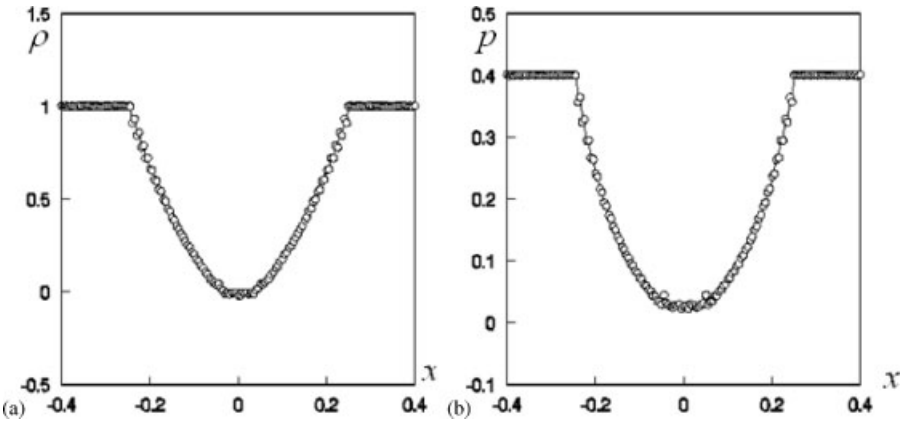

Figure 9. Comparison of the exact solution and the LBM results of one-dimensional Roe problem with a near-vacuum region. Solid lines are exact solutions, and circles are LBM results: (a) density and (b) pressure. The parameters are $\gamma=1.4, c=3.0, \tau=1.31, \varepsilon_A=6.5c^2, \varepsilon_B=2.0c^2, \varepsilon_D=0.02c^2, \widetilde{k}=k$, the lattice size is 200, and time $t=50\Delta t$. The variables P' and R' are computed by using first-order difference schemes (84)–(85).

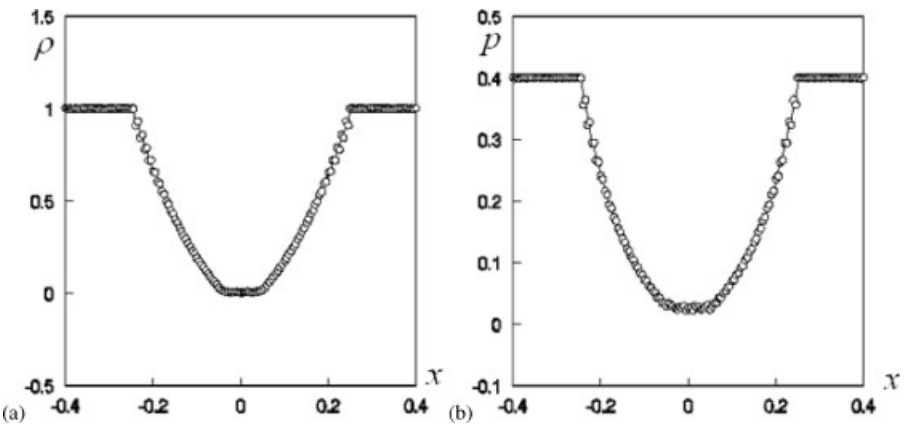

Figure 10. Comparison of the exact solution and the LBM results of one-dimensional Roe problem with a near-vacuum region. Solid lines are exact solutions, and circles are LBM results: (a) density and (b) pressure. The parameters are $\gamma=1.4, c=3.0, \tau=1.31, \varepsilon_A=6.5c^2, \varepsilon_B=2.0c^2, \varepsilon_D=0.02c^2, \widetilde{k}=0.1k$, the lattice size is 200, and time $t=50\Delta t$. The variables P' and R' are computed by using second-order difference schemes (86)–(87).

is the same as the schemes STGU and STGC. We note that when this model is applied to the Roe problem, the results are better than the results in Reference [28]. The 'tip' in the contact interface in the Roe problem case I is polished, and the model can restrain the negative value automatically in the near-vacuum region in the Roe problem case II.

DOI: 10.1002/fld

Table I. L_1 norm errors of the Sod problem and the Lax problem.

	The Sod problem ($t=0.1644$), lattice size=200			The Lax problem ($t=0.16$), lattice size$=200$		
	Density	Velocity	Pressure	Density	Velocity	Pressure
Reference [28]	0.00804	0.01673	0.00792	0.03051	0.01937	0.04901
Reference [30]	0.00521	0.00852	0.00376	0.01622	0.01205	0.01403
This model with first-order difference scheme	0.00509	0.00784	0.00427	0.01486	0.01321	0.01336
This model with second-order difference scheme	0.00193	0.00334	0.00251	0.00545	0.01086	0.00923
LxF	0.01769	0.02814	0.01582	0.06165	0.05557	0.06537
ORD	0.00578	0.00959	0.00460	0.02231	0.01709	0.01995
ULT1	0.00437	0.00820	0.00362	0.01477	0.01049	0.01206
STG2	0.00297	0.00494	0.00228	0.01151	0.00849	0.00988
STGU	0.00291	0.00403	0.00216	0.01302	0.01306	0.01121
STGC	0.00172	0.00276	0.00153	0.00647	0.00836	0.00823
ULTC	0.00361	0.00804	0.00362	0.00872	0.01074	0.01183
ROE	0.00836	0.01145	0.00666	0.02827	0.02192	0.02655

These results come from Reference [39], except three LBM results. The underlined results indicate the smallest L_1 norm errors in every column.

5. CONCLUSIONS

In this paper, we proposed a new lattice Boltzmann model for the compressible Euler equations. The new model is based on a three-energy-level and three-speed lattice Boltzmann equation by using a method of higher moments of the equilibrium distribution functions. In order to remove the terms $(\gamma-1)(3-\gamma)\rho E\partial u/\partial x$ and $(\gamma-1)(3-\gamma)\rho Eu\partial u/\partial x+\gamma(\gamma-1)\rho E\partial E/\partial x$, we put an additional distribution function, called the ghost field distribution function. As an essential step, the local ghost field equilibrium distribution must satisfy the conservation conditions and conditions of higher-order moments Equations (41)–(47).

In order to obtain the coefficients in the equilibrium distribution, we propose some man-made complementary conditions. It is a simple strategy to determine the coefficients that such assumptions are employed. Of course, the assumptions are not unique, and the effects of other artificial complementary conditions remain to be considered.

The main targets of the paper are listed as: (1) Instead of building an LBM for the Navier–Stokes equations, we propose a new lattice Boltzmann model for the second-order compressible Euler equations by using the ghost field. (2) We obtain the equilibrium distribution functions of the ghost field. It is the fundamental law that develops the lattice Boltzmann model for two- and three-dimensional Euler equations.

In this paper, we compare the numerical results with those obtained by traditional methods. Our model may not be a high-resolution scheme, but it is still attractive. This model preserves the main advantages of the available lattice Boltzmann model. If we apply classical high-resolution techniques to the LBM, the scheme could be an interesting one.

DOI: 10.1002/fld

Finally, we point out that some problems remain to be solved: (1) how to find the variables P' and R' computed by using the second-order difference scheme in two-dimensional models and (2) how to obtain the rule between the man-made complementary conditions (22) and (52)–(53) and the numerical results. We will discuss these problems in future papers.

ACKNOWLEDGEMENTS

This work is supported by the 985 Project of Jilin University, the National Nature Science Foundation of China (Grant Nos. 10072023 and 90305013), and the ChuangXin Foundation of Jilin University (No. 2004CX041). We would like to thank Prof. Hu Shouxin, Prof. Wang Jianping, Dr. Liu Yanhong, Dr. Wang Huimin and Dr. Yan Bo for their many helpful suggestions.

REFERENCES

1. Frisch U, Hasslacher B, Pomeau Y. Lattice gas automata for the Navier–Stokes equations. *Physical Review Letters* 1986; **56**:1505–1508.
2. Chen SY, Doolen GD. Lattice Boltzmann method for fluid flows. *Annual Review of Fluid Mechanics* 1998; **3**:314–322.
3. Qian YH, d'Humieres D, Lallemand P. Lattice BGK model for Navier–Stokes equations. *Europhysics Letters* 1992; **17**(6):479–484.
4. Chen HD, Chen SY, Matthaeus MH. Recovery of the Navier–Stokes equations using a lattice-gas method. *Physical Review A* 1992; **45**:5339–5342.
5. Benzi R, Succi S, Vergassola M. The lattice Boltzmann equation: theory and applications. *Physics Reports* 1992; **222**:147–197.
6. Yan GW. A lattice Boltzmann equation for waves. *Journal of Computational Physics* 2000; **161**:61–69.
7. Yan GW, Song M. Recovery of the solitons using a lattice Boltzmann model. *Chinese Physics Letters* 1999; **16**:109–110.
8. Yan GW, Yuan L. Lattice Bhatnagar–Gross–Krook model for the Lorenz attractor. *Physica D* 2001; **154**:43–50.
9. Zhang JY, Yan GW. Lattice Boltzmann method for one and two-dimensional Burgers equation. *Physica A*, DOI: 10.1016/j.physa.2008.04.002.
10. Zhang JY, Yan GW. A lattice Boltzmann model for the nonlinear Schrödinger equation. *Journal of Physics A* 2007; **40**:10393–10405.
11. Succi S. Numerical solution of the Schrödinger equation using discrete kinetic theory. *Physical Review E* 1996; **53**:1969–1975.
12. Wang MR, Wang JK, Chen SY. Roughness and cavitations effects on electro-osmotic flows in rough microchannels using the lattice the lattice Poisson–Boltzmann method. *Journal of Computational Physics* 2007; **226**:836–851.
13. Chai ZH, Shi BC. A novel lattice Boltzmann model for the Poisson equation. *Applied Mathematical Modelling* 2007; DOI: 10.1016/j.apm.2007.06.033.
14. Alexander FJ, Chen H, Chen S *et al*. Lattice Boltzmann model for compressible fluids. *Physical Review A* 1992; **46**:1967–1970.
15. Nadiga BT. An Euler solver based on locally adaptive discrete velocities. *Journal of Statistical Physics* 1995; **81**:129–146.
16. Huang J, Xu F, Vallieres M *et al.* A thermal LBGK model for large density and temperature difference. *International Journal of Modern Physics C* 1997; **8**:827–841.
17. Prendergast KH, Xu K. Numerical hydrodynamics from gas-kinetic theory. *Journal of Computational Physics* 1993; **109**:53–66.
18. Kim C, Xu K, Martinelli L *et al*. Analysis and implementation of the gas kinetic BGK scheme for computing inhomogeneous fluid behavior. *International Journal for Numerical Methods in Fluids* 1997; **25**:21–49.
19. Kotelnikov AD, Montgomery DC. A kinetic method for computing inhomogeneous fluid behavior. *Journal of Computational Physics* 1997; **134**:364–388.
20. Renda A, Bella G, Succi S *et al*. Thermo hydrodynamics lattice BGK schemes with non-perturbative equilibrium. *Europhysics Letters* 1998; **41**:279–283.

21. Vahala G, Pavlo P, Vahala L *et al*. Thermal lattice Boltzmann models (TLBM) for compressible flows. *International Journal of Modern Physics C* 1998; **9**:1247–1261.
22. Sun CH. Lattice-Boltzmann model for high speed flows. *Physical Review E* 1998; **58**:7283–7287.
23. De Cicco M, Succi S, Bella G. Nonlinear stability of compressible thermal lattice BGK model. *SIAM Journal on Scientific Computing* 1999; **21**:366–377.
24. Mason RJ. A compressible lattice Boltzmann model. *Bulletin of the American Physical Society* 2000; **45**:168–170.
25. Mason RJ. A multi-speed compressible lattice Boltzmann model. *Journal of Statistical Physics* 2002; **107**: 385–400.
26. Kataoka T, Tsutahara M. Lattice Boltzmann method for the compressible Euler equations. *Physical Review E* 2004; **69**(5):Art No. 056702.
27. Kataoka T, Tsutahara M. Lattice Boltzmann method for the compressible Navier–Stokes equations with flexible specific-heat ratio. *Physical Review E* 2004; **69**(3):Art No. 035701.
28. Yan GW, Chen YS, Hu SX. Simple lattice Boltzmann model for simulating flows with shock wave. *Physical Review E* 1999; **59**:454–459.
29. Yan GW, Dong YF, Liu YH. An implicit Lagrangian lattice Boltzmann method for the compressible flows. *International Journal for Numerical Methods in Fluids* 2006; **51**:1407–1418.
30. Yan GW, Zhang JY, Liu YH, Dong YF. A multi-energy-level lattice Boltzmann model for the compressible Navier–Stokes equations. *International Journal for Numerical Methods in Fluids* 2007; DOI:10.1002/fld.1440.
31. Versteeg HK, Malalasekera W. *An Introduction to Computational Fluid Dynamics—The Finite Volume Method*. Longman Group Ltd, 1995.
32. Harten A. On a class of high resolution total variation stable finite difference schemes. *SIAM Journal on Numerical Analysis* 1984; **21**:1–23.
33. Harten A, Engquist B, Osher S, Chakravathy R. Uniformly high order accurate essentially non-oscillatory schemes III. *Journal of Computational Physics* 1997; **131**:3–47.
34. Zhang LT, Wagner GJ, Liu WK. A parallelized meshfree method with boundary enrichment for large-scale CFD. *Journal of Computational Physics* 2002; **176**:483–506.
35. Sethian JA. Theory, algorithms, and applications of level set methods for propagating interface. *Acta Numerica*. Cambridge University Press: Cambridge, U.K., 1995.
36. Succi S, Benzi R, Cali A, Vergassola M. The lattice Boltzmann equation: theory and application. In *Microscopic Simulations of Complex Hydrodynamic Phenomena*, Mareschal M, Holian BL (eds). Plenum Press: New York, 1992; 187–203.
37. Chapman S, Cowling TG. *The Mathematical Theory of Non-uniform Gas*. Cambridge University Press: Cambridge, 1939.
38. Yan GW, Yuan L. Lattice Boltzmann model for the perfect gas flows with near-vacuum region. *Communication in Nonlinear Science and Numerical Simulation* 2000; **5**(2):58–63.
39. Nessyahu H, Tadmor E. Non-oscillatory central differencing for hyperbolic conservation laws. *Journal of Computational Physics* 1990; **87**:408–419.